Anisotropy of MHD turbulence at low magnetic Reynolds number

By O. Zikanov and A. Vorobev †, A. Thess ‡ P. A. Davidson ¶ AND B. Knaepen ||

Turbulent fluctuations in MHD flows are known to become dimensionally anisotropic under the action of a sufficiently strong magnetic field. We consider the technologically relevant case of low magnetic Reynolds number and apply the method of DNS of forced flow in a periodic box to generate velocity fields. The analysis based on different anisotropy characteristics shows that the dimensional anisotropy is virtually scale-independent. We also find that, except for the case of very strong magnetic field, the flow is componentally isotropic. Its kinetic energy is practically uniformly distributed among the velocity components.

1. Introduction

Magnetohydrodynamic (MHD) turbulent flows are ubiquitous in the universe, occurring in numerous astrophysical, geophysical, and technological applications. It is known that in the presence of a sufficiently strong magnetic field the turbulent fluctuations become anisotropic, which implies important consequences for the properties of the turbulence and possibly requires modification of numerical models. Specific manifestation of the anisotropy may vary but the principal mechanism is always the elongation of flow structures (turbulent eddies) along the lines of the magnetic field.

The main difference between the kinds of MHD turbulence is due to different values of the magnetic Reynolds number

$$\mathrm{Re}_m \equiv \frac{uL}{\eta}, \tag{1.1}$$

where $\eta = (\sigma\mu_0)^{-1}$ is the magnetic diffusivity, σ and μ_0 being the electric conductivity of the liquid and magnetic permeability, and u, L are the typical velocity and length scales of the flow. If $\mathrm{Re}_m > 1$, there is a two-way coupling between fluctuations of magnetic field and velocity. This happens in astrophysical applications (stars, interstellar medium, etc.), where $\mathrm{Re}_m \gg 1$, and in geophysical applications (Earth dynamo), where Re_m is smaller but still significantly larger than 1. Discussions of anisotropy effects at large magnetic Reynolds number can be found, for example, in the recent review by Cho *et al.* (2002).

The opposite case of $\mathrm{Re}_m \ll 1$ occurs in a majority of technological processes, where a strong steady magnetic field is imposed on an electrically conducting liquid. Examples of such applications include continuous casting of steel and aluminum, growth of semiconductor crystals, and lithium cooling blankets for fusion reactors. In this case, the low-Re_m (so-called quasi-static) approximation can be applied (see, e.g., Moreau 1990 or

† University of Michigan - Dearborn
‡ Ilmenau University of Technology
¶ University of Cambridge
|| Universite Libre de Bruxelles

Davidson 2001). It can be assumed that the fluctuations of the magnetic field **b** associated with fluid motions adjust instantaneously to the velocity fluctuations and that their amplitude is negligible in comparison with the amplitude of imposed magnetic field **B**. The rotational part of the Lorentz force reduces to the linear functional of the velocity

$$\mathbf{F}[\mathbf{v}] = -\frac{\sigma B^2}{\rho}\triangle^{-1}\frac{\partial^2 \mathbf{v}}{\partial z^2}, \tag{1.2}$$

where ρ and $\mathbf{u}$ are the density and velocity of the fluid, $\triangle^{-1}$ is the reciprocal Laplace operator, and we assumed that the imposed magnetic field is uniform and purely vertical $\mathbf{B} = B\mathbf{e}_z$.

The flow transformation under the impact of force (1.2) has been actively studied in analytical (Moffatt 1967, Sommeria & Moreau 1982, Davidson 1997, 1999), experimental (Votsish & Kolesnikov 1976, Alemany *et al.* 1979) and numerical (Schumann 1976, Zikanov & Thess 1998) works. The papers mentioned above represent only a fraction of the literature on the subject, more references being available therein. Far from the walls, the action of the magnetic field was identified as two-fold. First, the induced electric currents result in additional dissipation of kinetic energy, the Joule (magnetic) dissipation. Second, the flow becomes anisotropic, its structures being elongated along the magnetic field lines.

The reason for the anisotropy becomes especially transparent if one assumes that the flow is unbounded and uniform and uses the Fourier representation.† The Fourier transform of (1.2) is

$$\widehat{\mathbf{F}}[\widehat{\mathbf{v}}] = -\frac{\sigma}{\rho}\frac{(\mathbf{B}\cdot\mathbf{k})^2}{k^2}\widehat{\mathbf{v}}(\mathbf{k},t) = -\frac{\sigma B^2}{\rho}\widehat{\mathbf{v}}(\mathbf{k},t)\cos^2\theta, \tag{1.3}$$

where $\mathbf{k}$ is the wavenumber vector and θ is the angle between $\mathbf{k}$ and $\mathbf{B}$. The rate of Joule dissipation of a Fourier mode with the wavenumber vector $\mathbf{k}$ is

$$\mu(\mathbf{k}) = \frac{\sigma B^2}{\rho}(\widehat{\mathbf{v}}(\mathbf{k},t)\cdot\widehat{\mathbf{v}^*}(\mathbf{k},t))\cos^2\theta, \tag{1.4}$$

so the dissipation is anisotropic. It attains maximum for the Fourier modes with $\mathbf{B} \parallel \mathbf{k}$ and zero for modes with $\mathbf{B} \perp \mathbf{k}$, i.e., for modes independent of the z-coordinate. The dissipation tends to eliminate the velocity gradients in the direction of $\mathbf{B}$ and elongate the flow structures in this direction. The limiting case is the two-dimensional state completely independent of the z-coordinate. The Joule dissipation is equal to zero in this state.

This picture of the flow transformation was first given by Moffatt (1967) and later beautifully illustrated by Sommeria & Moreau (1982), who introduced the image of 'Joule cone' in the wavenumber space around the $\mathbf{B}$-direction, in which the magnetic dissipation takes place. A remarkable feature of the picture is that, according to (1.4), the relative rate of the dissipation $\mu(\mathbf{k})/\widehat{\mathbf{u}}^2$ depends on the angle θ but not on the wavenumber k. One can, thus, assume that the anisotropy would develop equally on all length scales of the flow.

The situation, however, looks much more complicated if one takes into account the non-linearity of the Navier-Stokes equations and the resulting energy transfer between the modes and tendency to restoration of isotropy. The ratio between the Lorentz force

† The process of development of anisotropy can be viewed from a different angle. In particular, Davidson (1997) proposed a scenario based on the fact that the Lorentz force conserves momentum component parallel to the magnetic field.

and non-linear term is evaluated by the magnetic interaction parameter (Stuart number)

$$\mathrm{N} \equiv \frac{\sigma B^2 L}{\rho u}. \tag{1.5}$$

It is clear that the linearized picture of the flow development discussed above is true only in the limit of $\mathrm{N} \gg 1$. At finite N, one can expect a more complex scenario, probably with scale-dependent anisotropy. In particular, the analogy with stratified, rotating, or strained turbulence (see, e.g., Smith & Moum 2000) suggests that smaller scales are more isotropic than large scales. Another way to arrive to the suggestion is to notice that, while the Joule damping time $\tau \equiv \rho/\sigma B^2$ is scale-independent, the eddy turnover time $T = L/u$ is not. The magnitude of the scale-related Stuart number $N = T/\tau$ can vary with the scale and so is the flow's anisotropy.

The question of anisotropy at different length scales is particularly important in the view of recent attempts to apply the traditional LES models to the low-Re_m MHD turbulence (Knaepen & Moin 2004). The a-posteriori evaluation of the dynamic model (Germano *et al.* 1991) showed good accuracy for decaying turbulence at moderate hydrodynamic Reynolds number and $\mathrm{N} \leq 10$. This result is counter-intuitive since one expects LES models developed in assumption of local isotropy to perform poorly in the case of strongly anisotropic flow. One can not guarantee that equally good results will be obtained at higher Reynolds numbers.

In this paper, we investigate the anisotropy of low-Re_m MHD turbulence using the DNS of forced flow in a box with periodic boundary conditions. The model and the numerical experiments are described in section 2. Various measures of anisotropy are discussed and evaluated in section 3. Possible implications for LES subgrid-scale modeling are discussed in section 4. Finally, summary and concluding remarks are provided in section 5.

2. Model and numerical experiments

We solve MHD equations for viscous, incompressible and electrically-conducting fluid in the quasi-static approximation. The Lorentz force term is given by (1.2). After applying $(\nabla\times)\times$ operation to eliminate pressure and taking Fourier transform, the governing equation become

$$\frac{\partial \hat{\mathbf{v}}}{\partial t}(\mathbf{k},t) = -\frac{1}{k^2}[\mathbf{k}\times(\mathbf{k}\times\hat{\mathbf{q}})] - \left[\nu\mathbf{k}^2 + \frac{\sigma B_0^2}{\rho}\left(\frac{k_z}{k}\right)^2\right]\hat{\mathbf{v}}, \tag{2.1}$$

where ν is the kinematic viscosity and $\hat{\mathbf{q}}$ is the Fourier transform of the nonlinear term. The incompressibility condition used in derivation of (2.1) can be applied to recover the modified pressure field. A statistically homogeneous flow is calculated within a rectangular box with periodical boundary conditions. Since we expect axial anisotropy of turbulent flow, and elongation of turbulent vortexes along the z-axis, the elongated box of dimensions $2\pi \times 2\pi \times 4\pi$ is used. The equation (2.1) is solved by the standard pseudo-spectral technique.

In order to generate a statistically steady flow over long period of time, an artificial forcing is applied at large length scales. A constant amount of energy is added at each time-step. When equilibrium is reached the amount of energy added is on average equal to the energy dissipated. The external force

$$\mathbf{H}(\mathbf{k}) = \alpha(\mathbf{k})\hat{\mathbf{v}}(\mathbf{k}) \tag{2.2}$$

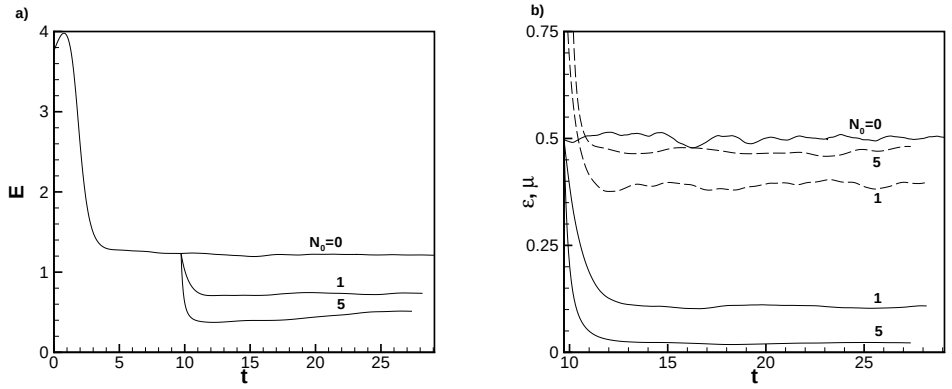

FIGURE 1. *(a)*, Evolution of total energy. *(b)*, Evolution of rates of total viscous (——) and magnetic (– – –) dissipation.

is applied to modes with $1.5 \leq k \leq 3.1$. The time-dependent coefficients α are determined so that the net work by forcing is equal to the prescribed total (viscous and magnetic) rate of dissipation ϵ_0 and the work is equally divided among the forced modes

$$\alpha(\mathbf{k}) = \frac{\epsilon_0}{N_{forced}(\hat{\mathbf{v}}(\mathbf{k}) \cdot \hat{\mathbf{v}}^*(\mathbf{k}))}, \tag{2.3}$$

where N_{forced} is the number of forced modes and * stands for complex conjugate.

Simulations are performed with numerical resolution $256 \times 256 \times 512$. The parameters $\epsilon_0 = 0.5$ and $\nu = 2.2 \cdot 10^{-3}$ are chosen so as to guarantee the accuracy criterion $k_{max}\eta > 1.5$, where k_{max} is the maximum resolved wavenumber and η is the Kolmogorov dissipation scale. The microscale Reynolds number is $\mathrm{Re}_\lambda \approx 94$ in the non-magnetic run.

The numerical experiments are staged as illustrated in figure 1. First, a developed turbulent flow is calculated starting with random, isotropic, and homogeneous field and continuing simulations without magnetic field for sufficiently long period. The completeness of the transitional period is judged by stabilization of the values of the total kinetic energy, viscous and magnetic dissipation rates defined as

$$E = \frac{1}{2}\sum_{\mathbf{k}} \left(\mathbf{v}(\mathbf{k}) \cdot \mathbf{v}^*(\mathbf{k})\right), \quad \epsilon = \nu \sum_{\mathbf{k}} k^2 \left(\mathbf{v}(\mathbf{k}) \cdot \mathbf{v}^*(\mathbf{k})\right), \quad \mu = \frac{\sigma B_0^2}{\rho} \sum_{\mathbf{k}} \frac{k_z^2}{k^2} \left(\mathbf{v}(\mathbf{k}) \cdot \mathbf{v}^*(\mathbf{k})\right). \tag{2.4}$$

The flow field computed at the moment $t_0 = 9.72$ is used as an initial condition for three simulations with different strength of the magnetic field. At $t = t_0$, the integral length scale is $L = 0.73$ and the rms turbulent velocity is $u = 0.71$, which gives the turbulent eddy turnover time of about 1. The strength of magnetic field in each run can be identified by the values of magnetic interaction parameter (1.5) at $t = t_0$. The cases with no magnetic field ($N_0 = 0$), moderate magnetic field ($N_0 = 1$), and strong magnetic field ($N_0 = 5$) are considered†.

A comment must be made regarding the limitations of the traditional DNS approach that can affect the accuracy of our results. First, at moderate Re_λ, the artificial forcing can have some impact on a significant portion of the resolved length scales. Second

† The flow evolution caused by magnetic field leads to significant increase of N during the runs (to about 1.2 in the second case and 10 in the third case).

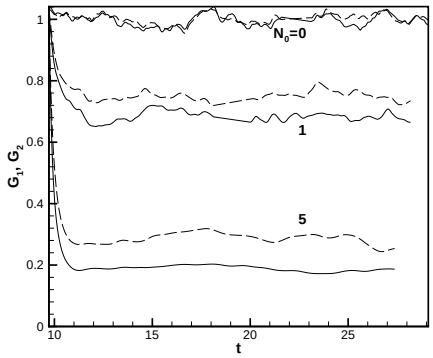

FIGURE 2. Anisotropy coefficients G_1 (——) and G_2 (– – –) given by (2.6).

(perhaps less important for us here), the integral length scale is relatively large (about 1/5 of the box size at $t = t_0$). The periodic boundary conditions can, therefore, affect the flow behavior at largest scales.

The evolution of total energy, viscous and magnetic dissipation is shown in figure 1. It can be seen that the period of adjustment after the introduction of magnetic field lasts several turnover times, after which the flow behavior is statistically steady. In the flows with magnetic field, the Joule dissipation is responsible for major part of the total dissipation rate $\epsilon_0 = \epsilon(t) + \mu(t)$.

Zikanov & Thess (2004) proposed using anisotropic Taylor microscales

$$\lambda_i \equiv \left[\frac{\langle v_j^2 \rangle}{(1+\delta_{ij})\langle (\partial v_j/\partial x_i)^2 \rangle} \right]^{1/2} \tag{2.5}$$

as global measures of anisotropy of velocity gradients. Here, any velocity component v_i can be used and $\langle \cdots \rangle$ stands for volume averaging. For isotropic turbulence, λ_i are all statistically equal to the usual Taylor microscale $\lambda = [15\nu u^2/\epsilon]^{1/2}$. The ratio $(\lambda_\perp/\lambda_\parallel)^2$ of length scales measured in the directions transverse and parallel to the magnetic field is equal to often used anisotropy coefficients (see, e.g., Schumann 1976 or Zikanov & Thess 1998) shown in figure 2

$$G_1 = \frac{\left\langle (\partial v_2/\partial z)^2 \right\rangle}{2\left\langle (\partial v_2/\partial y)^2 \right\rangle}, \quad G_2 = 2\frac{\left\langle (\partial v_3/\partial z)^2 \right\rangle}{\left\langle (\partial v_3/\partial y)^2 \right\rangle}. \tag{2.6}$$

Figure 3 shows skewness and flatness of longitudinal derivatives of the velocity components

$$S_i = -\frac{\left\langle (\partial v_i/\partial x_i)^3 \right\rangle}{\left\langle (\partial v_i/\partial x_i)^2 \right\rangle^{3/2}}, \quad F_i = \frac{\left\langle (\partial v_i/\partial x_i)^4 \right\rangle}{\left\langle (\partial v_i/\partial x_i)^2 \right\rangle^2}. \tag{2.7}$$

In the isotropic flow at $N_0 = 0$, all three components of skewness and flatness are approximately equal to $S \approx 0.5$ and $F \approx 5.4$. In the presence of magnetic field, the components measured across and along the magnetic field differ considerably. For skewness, the transverse components remain close to the isotropic value, although some drop can be seen in

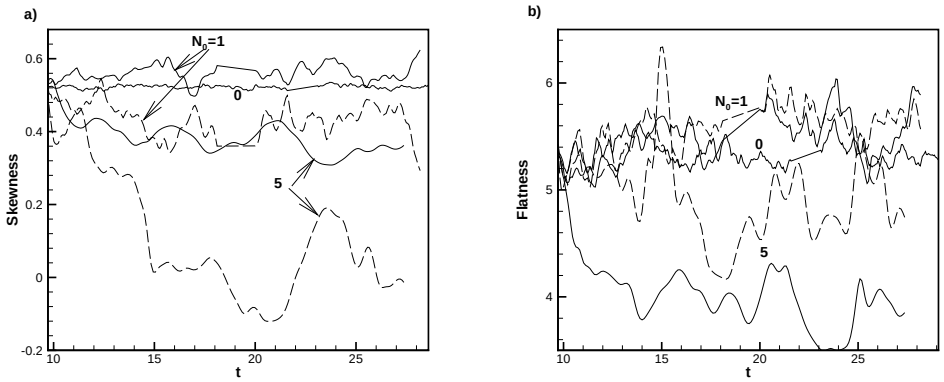

FIGURE 3. Skewness *(a)* and flatness *(b)* coefficients (2.7) measured across ($(S_1 + S_2)/2$ and $(F_1 + F_2)/2$ shown as ——) and along (S_3 and F_3 shown as – – –) magnetic field. For $N_0 = 0$, solid lines show $(S_1 + S_2 + S_3)/3$ and $(F_1 + F_2 + F_3)/3$.

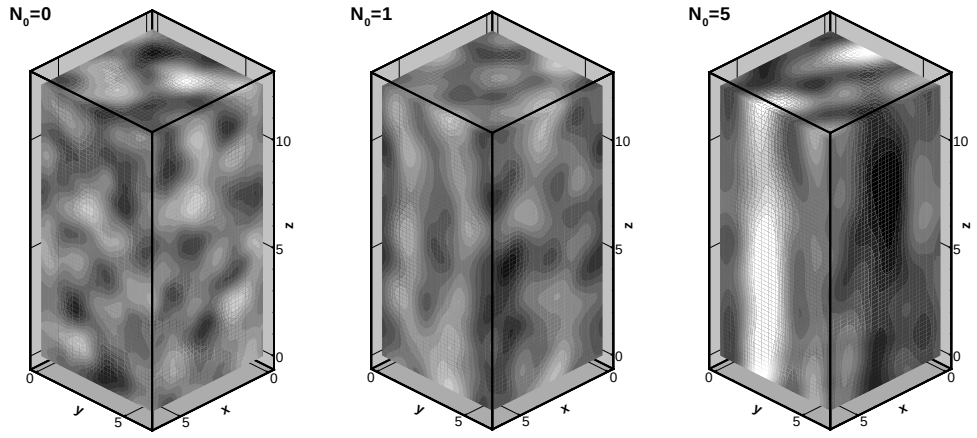

FIGURE 4. Modified pressure fields in developed flows.

the case of $N_0 = 5$. The parallel component decreases significantly at $N_0 = 1$ and even more so at $N_0 = 5$. This clearly indicates suppression of nonlinear energy transfer and dissipation of strong longitudinal velocity gradients by the magnetic field. For flatness, we also observe significant reduction in the case of $N_0 = 5$, more pronounced for the transverse component.

The internal structure of flow field is illustrated in figure 4, where we show snapshots of modified pressure field made in developed flows at different magnetic field. The tendency to anisotropy is clearly seen, although even at $N_0 = 5$ the flow is far from approaching two-dimensional form.

The last issue to be discussed in this section is that of componental anisotropy, which is understood as anisotropy of the Reynolds stress tensor or velocity field (Kassinos *et al.* 2001). As the Joule dissipation directly affects only velocity gradients along the magnetic field lines, the componental anisotropy is a secondary effect, which existence and strength

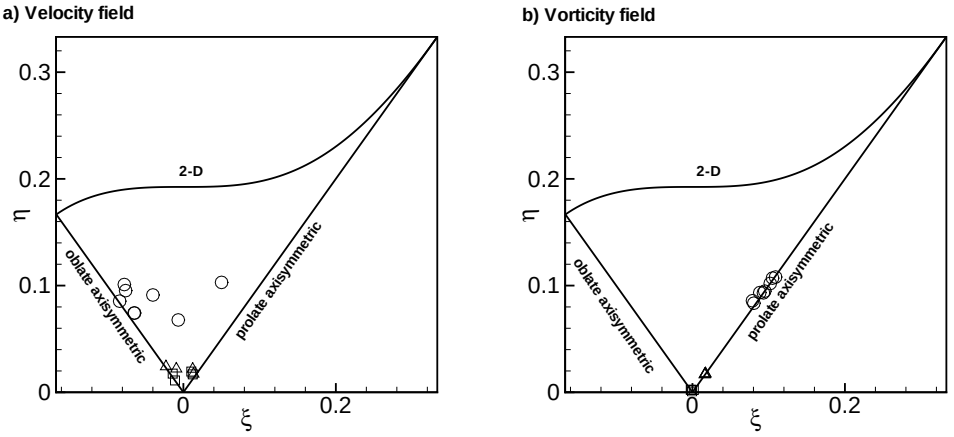

FIGURE 5. Invariant maps for componental anisotropy of velocity *(a)* and vorticity *(b)* fields. Squares, triangles, and circles are for $N_0 = 0$, 1, and 5, correspondingly.

is far from being obvious. The componental anisotropy of field $\mathbf{v}$ is traditionally evaluated with the help of the traceless tensor (Lumley & Newman 1977)

$$b_{ij} = \frac{\langle v_i v_j \rangle}{\langle v_k v_k \rangle} - \frac{1}{3}\delta_{ij}, \tag{2.8}$$

which has two nontrivial invariants $6\eta^2 = b_{ij}b_{ji}$ and $6\xi^3 = b_{ij}b_{jk}b_{ki}$. The magnitude of η represents the degree of anisotropy, with $\eta = 0$ for an isotropic flow, and the upper boundary $\eta = \left(1/22 + 2\xi^3\right)^{1/3}$ corresponding to a purely two-component case. The type of the anisotropy is determined by the sign of ξ. If $\xi > 0$, the flow is dominated by the velocity component parallel to the axis of symmetry (so-called prolate axisymmetric flow). Negative values of ξ mean domination of two perpendicular components (oblate axisymmetric flow).

We calculated the invariants at several time moments separated by few eddy turnover times. The results presented on the invariant map in figure 5a show that the velocity fields at $N_0 = 0$ and $N_0 = 1$ are fairly isotropic. The flow with strong magnetic field at $N_0 = 5$ demonstrates a degree of anisotropy. It is interesting that the velocity field migrates from being dominated by two velocity components perpendicular to the magnetic field to being dominated by one parallel component. This behavior can be associated with slow transformation of the large-scale structures of the flow.

We also calculated tensor (2.8) and invariants η and ξ for the vorticity field. The results shown in figure 5b are easy to explain. As the vertical gradients of velocity are eliminated in flows with higher N, the vorticity field becomes dominated by the vertical component.

3. Anisotropy at different length scales

In this section we analyze the calculated flow fields to determine how and whether at all the dimensional anisotropy varies with the length scale. We start with the power spectra shown in figure 6. The steepening of the energy spectrum and accompanying decrease of viscous dissipation are well known phenomena associated with the anisotropy (see, e.g., experiments by Alemany *et al.* 1979 or simulations by Zikanov & Thess 1998).

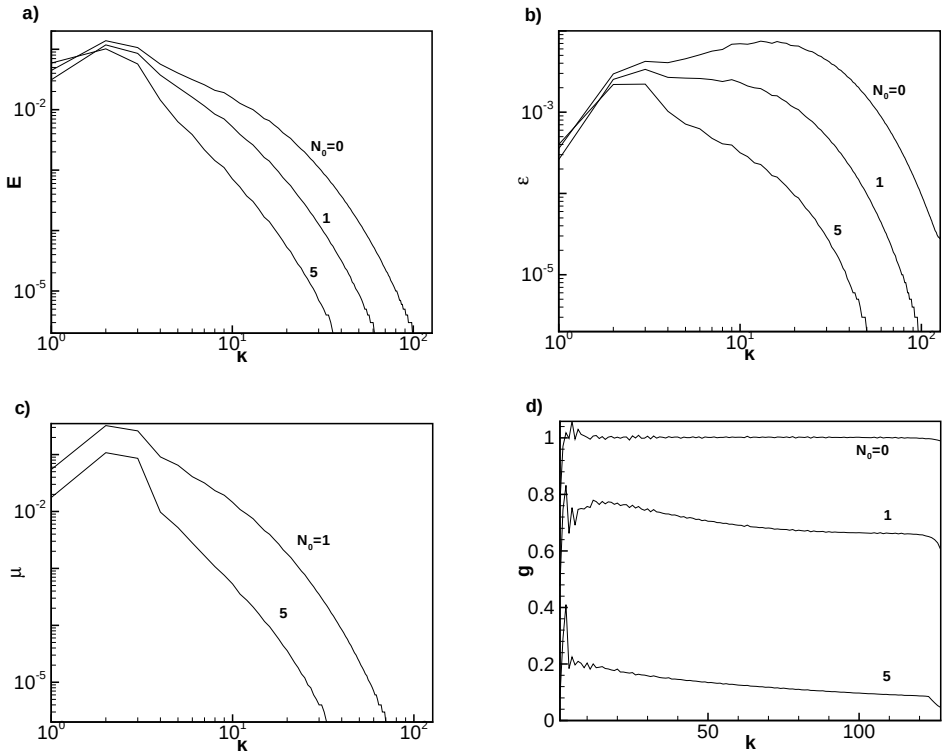

FIGURE 6. Spectra of *(a)* kinetic energy, *(b)* rate of viscous and *(c)* magnetic dissipation, and *(d)* spectra of anisotropy coefficient (3.1).

More interesting is the fact that the slope of Joule dissipation curves in figure 6c closely follows the slope of kinetic energy curves. This behavior detected earlier by Zikanov & Thess (1998) and confirmed here for larger Reynolds number gives, at least, a partial answer to our question. The ratio

$$g(k) \equiv \frac{3T_J}{2}\frac{\mu(k)}{E(k)} = \frac{3\sum \frac{k_z^2}{k^2}\hat{\mathbf{u}}\cdot\hat{\mathbf{u}}^*}{\sum \hat{\mathbf{u}}\cdot\hat{\mathbf{u}}^*} = \frac{3D_{33}(k)}{2E(k)} \tag{3.1}$$

can be considered as a measure of dimensional anisotropy at the wavelength k. In (3.1), the sum is over all wavenumber vectors in the shell $k-1/2 < |\mathbf{k}| \le k+1/2$, $T_J = \rho/\sigma B^2$ is the Joule dissipation time, and D_{33} is the component of the dimensionality tensor considered by Kassinos *et al.* (2001). The scaling factor is chosen so as to provide $g = 1$ in an isotropic flow. It can be seen in figure 6d that, outside of the forced region, $g(k)$ varies only slightly with k both at moderate and strong magnetic field. Even this slight decrease can be attributed to the effect of forcing. The magnitude of $g(k)$ is close to that of the global anisotropy coefficients G_1 and G_2 shown in figure 2.

The use of Fourier wavenumbers is arguably not the best way to consider the length scale decomposition of the flow properties. In the following we concentrate on analyzing the flow anisotropy in the physical space. First, figures 7 and 8 show the two-point velocity correlations along the direction perpendicular and parallel to the magnetic field. For the correlations in figure 7 we assume axial symmetry and calculate, for example,

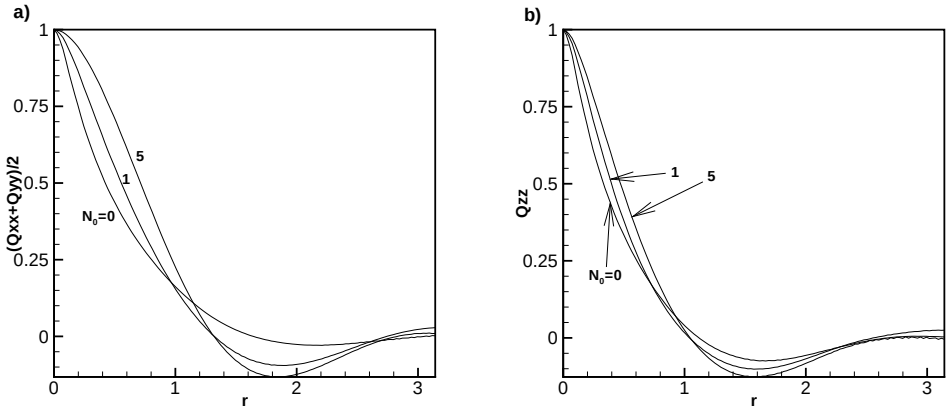

FIGURE 7. Correlations of velocity field in the direction perpendicular to the magnetic field.

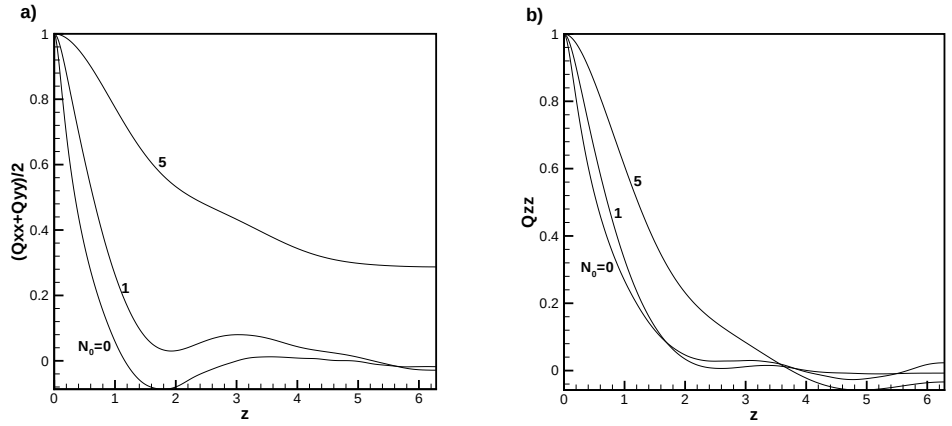

FIGURE 8. Correlations of velocity field in the direction parallel to the magnetic field.

$Q_{xx} = \langle u(\mathbf{x})u(\mathbf{x}+r\mathbf{e}_\perp)\rangle/\langle u^2\rangle$, where $\langle\cdots\rangle$ now stands for space averaging in $\mathbf{x}$ and averaging over all horizontal directions of $\mathbf{e}_\perp$.

One can see in figures 7 and 8 that imposing a magnetic field leads to growth of correlations not only in parallel but also in perpendicular direction. This is in agreement with the development of larger coherent structures in this case (see figures 4). Interestingly, as can be seen from comparison of plots *(a)* and *(b)* in both figures, the vertical velocity component experience much smaller increase than the horizontal components.

Figure 9 can be considered a physical-space analog of figure 6d. We calculate the second-order structure functions $\Upsilon_i(r) \equiv \langle (v_i(\mathbf{x}+r\mathbf{e}_i)-v_i(\mathbf{x}))^2\rangle$ and evaluate the anisotropy at the physical scale r as the ratio

$$R(r) = \frac{2\Upsilon_3}{\Upsilon_1+\Upsilon_2}. \tag{3.2}$$

One can see that, again, the anisotropy is virtually scale-independent.

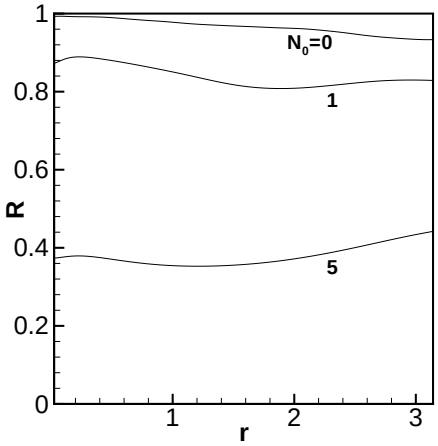

FIGURE 9. Anisotropy coefficient $R(r)$ given by (3.2).

4. Anisotropy of stress and strain tensors

One of the goals of this work is better understanding of properties of MHD flows related to the subgrid-scale turbulence modeling in LES. One can assume that the traditional SGS closures developed under the assumption of local isotropy are not suitable for strongly anisotropic MHD flows at high N. The opposite conclusion was made by Knaepen & Moin (2004) who performed LES of decaying turbulence at moderate Re and N up to 10. They found that the dynamic Smagorinsky model (Germano *et al.* 1991) is not less accurate for the MHD flows than for isotropic flows without magnetic field. Whether such a good performance is specific to the dynamic model and whether it is related to the scale-independence of anisotropy discussed above requires further investigation. So far, we have analyzed the computed data by calculating root-mean-squares of components of the Reynolds stress and rate of strain tensors of filtered velocity field

$$\tau_{ij} - \frac{\delta_{ij}}{3}\tau_{kk}, \text{ where } \tau_{ij} = \widehat{v_i v_j} - \widehat{v}_i \widehat{v}_j \tag{4.1}$$

and

$$S_{ij} = \frac{1}{2}\left(\frac{\partial \widehat{v}_i}{\partial x_j} + \frac{\partial \widehat{v}_j}{\partial x_i}\right). \tag{4.2}$$

Here, the $\widehat{\cdots}$ stands for Fourier cut-off filtering at a wavenumber k. The results are presented as functions of k in figure 10. We assume the axial symmetry and take the averages of statistically equal quantities. It can be seen that the rate of strain tensor becomes increasingly anysotropic with growing N. There is a significant and consistent difference between the amplitudes of, say, S_{12} and S_{13}. On the other hand, the components of the Reynolds stress tensor are virtually indistinguishable for any N and for any filter cut-off k.

5. Conclusions

We performed simulations of forced homogeneous turbulence in a low-Re_m MHD flow. Three numerical experiments with equal constant energy input but different strength of

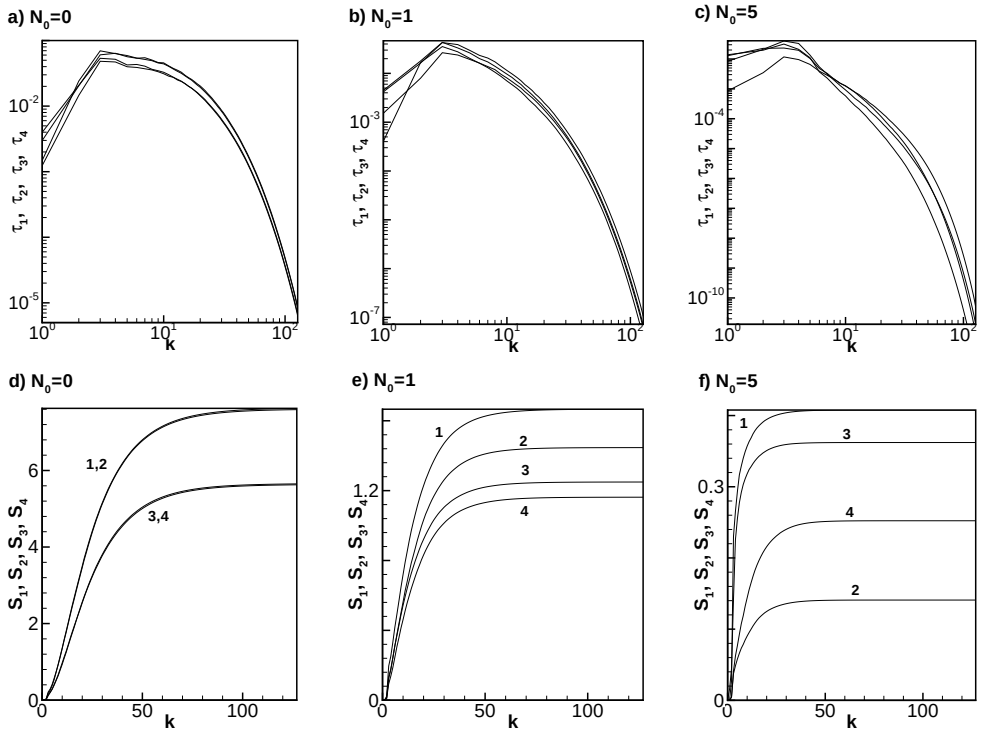

FIGURE 10. Spectra of root-mean squares of components of stress (top) and rate-of-strain (bottom) tensors of filtered velocity field as function of the filter cut-off k. Here $\tau_1 = \left\langle \tau_{11}^2 + \tau_{22}^2 \right\rangle /2$, $\tau_2 = \left\langle \tau_{33}^2 \right\rangle$, $\tau_3 = \left\langle \tau_{12}^2 + \tau_{21}^2 \right\rangle /2$, $\tau_4 = \left\langle \tau_{13}^2 + \tau_{31}^2 + \tau_{23}^2 + \tau_{32}^2 \right\rangle /4$. Similar notations used for rate-of-strain tensor. For $N_0 = 0$, τ_1 and τ_2 curves coalesce, as well as τ_3 and τ_4.

applied magnetic field were performed. The dimensional and componental anisotropy of the flow was analyzed both in the global sense and as a function of length scale. The main conclusions are as follows.

- While the flow develops strong dimensional anisotropy under the action of the Joule dissipation, its componental anisotropy remains insignificant. The kinetic energy remains approximately equally distributed over the velocity components.
- The analysis performed both in spectral and physical space showed that the dimensional anisotropy is virtually scale-independent. We can not exclude the possibility that different behavior can be observed at small scales of flows with much higher Reynolds numbers. On the other hand, the extent of the range of constant anisotropy was found to be quite significant in our simulations (about 2 orders of magnitude). We can consider the constancy a robust feature of low-Re_m MHD turbulence.

Part of this work was performed during the 2004 Summer Program at the Center for Turbulence Research with financial support from Stanford University and NASA Ames Research Center. The authors would like to thank P. Moin and N. Mansour for their hospitality during the stay. The authors have benefited from numerous fruitful discussions with R. Moreau, S. Kassinos, and D. Carati. AV's and OZ's work was supported by the grant DE FG02 03 ER46062 from the US Department of Energy. AT's work is

partially supported by the Deutsche Forschungsgemeinschaft in frame of the "Forschergruppe Magnetofluiddynamik" at Ilmenau University of Technology. OZ, AV and AT are grateful to the Deutscher Akademischer Austauschdienst and the National Science Science Foundation for financial support of their collaboration. The computations were performed on the NASA Ames parallel computers and on the parallel computer cluster at the University of Michigan - Dearborn acquired with the support of the grant CTS 0320621 from the MRI program of the National Science Foundation.

REFERENCES

ALEMANY A., MOREAU R., SULEM P.L, FRISCH U. 1979 Influence of external magnetic field on homogeneous MHD turbulence. *J. de Mecanique* **18**, 280–313.

CHO, J., LAZARIAN, A, VISHNIAC, E. T. 2002 MHD turbulence: Scaling laws and Astrophysical applications. *Astro-ph/0205286.*

DAVIDSON P.A. 1997 The role of angular momentum in the magnetic damping of turbulence. *J. Fluid Mech.* **336**, 123–150.

DAVIDSON P.A. 1999 Magnetohydrodynamics in Materials Processing. *Annu. Rev. Fluid Mech.* **31**, 273–300.

DAVIDSON P.A. 2001 An Introduction to Magnetohydrodynamics, *Cambridge University Press*, Cambridge.

GERMANO, M., PIOMELLI, U., MOIN, P., CABOT, W. H. 1991 A dynamic subgrid-scale eddy viscosity model. *Phys. Fluids* A **3**, 1760–1765.

KASSINOS, S. C., REYNOLDS, W. C., ROGERS, M. M. 2001 One-point turbulence structure tensors. *J. Fluid Mech.* **428**, 213–248.

KNAEPEN B., MOIN 2004 Large-eddy simulation of conductive flows at low magnetic Reynolds number. *Phys. Fluids* **16**, 1255–1261.

LUMLEY, J. L., NEWMAN, G. R. 1977 The return to anisotropy of homogeneous turbulence. *J. Fluid Mech.* **82**, 161–178.

MOFFATT H.K. 1967 On the suppression of turbulence by a uniform magnetic field. *J. Fluid Mech.* **28**, 571–592.

MOREAU R. 1990 Magnetohydrodynamics, *Kluwer Academic Publishers*, Dordrecht.

SCHUMANN U. 1976 Numerical simulation of the transition from three- to two-dimensional turbulence under a uniform magnetic field. *J. Fluid Mech.* **74**, 31–58.

SMITH, W. D. & MOUM, J. M. 2000 Anisotropy of turbulence in stably stratified mixing layers. *Phys. Fluids* **12**, 6, 1343–1362.

SOMMERIA J., MOREAU R. 1982 Why, how, and when, MHD turbulence becomes two-dimensional. *J. Fluid Mech.* **118**, 507–518.

VOTSISH, A. D. AND KOLESNIKOV, YU. B. 1976 Investigation of transition from three-dimensional turbulence to two-dimensional under a magnetic field. *Magn. Hydrodyn.* **3**, 141-142.

ZIKANOV O., A. THESS 1998 Direct numerical simulation of forced MHD turbulence at low magnetic Reynolds number. *J. Fluid Mech.* **358**, 299–333.

ZIKANOV O., A. THESS 2004 Direct numerical simulation as a tool for understanding MHD liquid metal turbulence. *Appl. Math. Mod.* **28**, 1–13.